Karlsruhe Institute of Technology

Silica in humid air environment:

(II): Diffusion under moderate stresses

Theo Fett[1], Sheldon M. Wiederhorn[2]

KIT SCIENTIFIC WORKING PAPERS 60

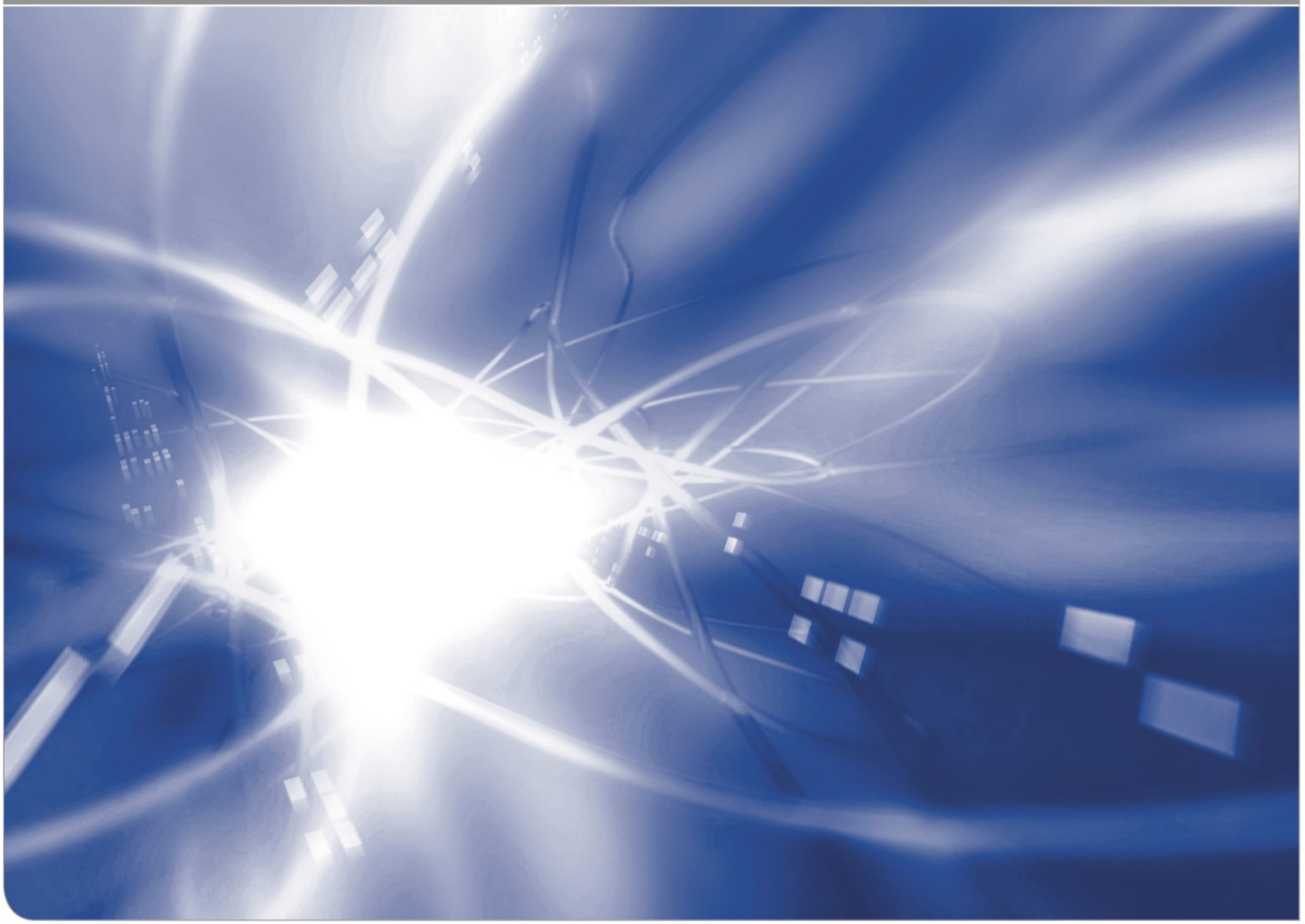

1) Karlsruhe Institute for Technology, Institute for Applied Materials

2) National Institute of Standards and Technology, Gaithersburg, MD

Impressum

Karlsruher Institut für Technologie (KIT)
www.kit.edu

2017

ISSN: 2194-1629

Abstract

Water diffusion into silica glass results in a thin zone near the surface of the glass. In this zone molecular and hydroxyl water are present. The content of hydroxyl water increases its specific volume so that the silica expands and the volume near the surface is larger than it was before being penetrated by the water. Suppressed free expansion of the glass causes biaxial compressive swelling stresses.

The effect of such swelling stresses and also of moderate externally applied stresses on the diffusion behaviour will be studied in this report for the case of a gaseous water environment at temperatures <500°C.

In the Appendix also the effect of stress-enhanced equilibrium constant is addressed and the behavior at higher temperatures briefly considered.

Contents

1. Water diffused into silica

When H_2O (l) comes in contact with silica surfaces, the water diffuses into the glass, and reacts with the silica network [1]

$$\equiv\text{Si-O-Si}\equiv + H_2O \leftrightarrow \equiv\text{SiOH+HOSi}\equiv \tag{1.1}$$

with the concentrations of molecular water, C=[H_2O], and hydroxyl water, S=[SiOH]. For the following considerations, it is assumed that the reaction (1.1) is in equilibrium. The equilibrium constant of the reaction (1.1) is at low temperatures, $T \leq 500°C$, represented by the ratio

$$k = \frac{S}{C} \tag{1.2}$$

The "water" concentration may be represented by the molecular water species, C.
In a previous report we have drawn attention to the fact that surface diffusion of water into silica can be described analytically by introducing mass transfer boundary conditions [2] or by a slow surface reaction according to Doremus [3].
This condition reads

$$\frac{dC}{dz} = -\frac{h}{D}(C_0 - C) \quad \text{at } z=0 \tag{1.3}$$

where z is the depth coordinate, C_0 the maximum content of molecular water reached at the surface, z=0, D the effective diffusivity, and h the mass transfer coefficient. The diffusion equation under reaction conditions follows from the motivation by Doremus [1] according to [4]

$$\frac{\partial C}{\partial t} = \frac{\partial}{\partial z}\left(D_C \frac{\partial C}{\partial z}\right) - \tfrac{1}{2}\frac{\partial S}{\partial t}$$

$$\overset{equilibrium}{\rightharpoonup\!\!\!\!\!\leftharpoondown} \quad \frac{\partial C}{\partial t} = \frac{\partial}{\partial z}\left(D \frac{\partial C}{\partial z}\right) \quad , D = \frac{D_C}{1+\tfrac{1}{2}k_0} \tag{1.4}$$

with the diffusivity D_C of molecular water, the effective diffusivity D for constant S/C and the equilibrium constant in the absence of stresses, k_0 (see also Appendix A1).
In [2] we applied eq.(1.4) for the special case of stress-independent diffusivity and equilibrium constant. In normal test specimens, the diffusion zones are very small compared to the specimen thickness. Under all these assumptions, the solution for the semi-infinite body reads according to Carslaw and Jaeger [5]

$$C(z)/C_0 = \operatorname{erfc}\left[\frac{z}{2\sqrt{Dt}}\right] - \exp\left[\frac{h}{D}z + \frac{h^2}{D}t\right]\operatorname{erfc}\left[\frac{z}{2\sqrt{Dt}} + h\sqrt{\frac{t}{D}}\right] \tag{1.5}$$

and for z=0:

$$C(0)/C_0 = 1 - \exp\left[\frac{h^2}{D}t\right]\mathrm{erfc}\left[h\sqrt{\frac{t}{D}}\right] \tag{1.6}$$

In the present report stress effects are included.

2. Swelling stresses

Clear evidence has been given in the literature for a volume swelling due to the water uptake in silica. Swelling of water-containing silica at high temperatures was reported by Shelby [6]. Since the measurements were performed at 1100°C, no molecular water was involved, only ≡SiOH. As pointed out in [7], the related volume swelling strain ε_v can be written in this special case as

$$\varepsilon_v \cong 1.84 C_w \tag{2.1}$$

where C_w is the *total* water concentration in the silica glass in mass units (g H_2O/g glass). By curvature measurements on silica disks it could be shown that the water penetrated into the silica surface caused volume expansion accompanied by compressive swelling stresses [8]. In the present report it is checked whether the swelling stresses can explain several interesting experimental results known from literature. As outlined in [9] the volume swelling strain is related to the hydroxyl concentration by

$$\varepsilon_v = \tfrac{18}{17}(1+\chi)\frac{S}{2} = \kappa \times S \tag{2.2}$$

with the coefficient

$$\kappa = 0.97 \;\; [0.92, 1.02] \tag{2.3}$$

The numbers in brackets represent the 95% confidence interval.
A volume element in a plate that undergoes swelling cannot freely expand. If the diffusion zone is small compared to the component dimensions; expansion is completely prevented in the plane of the surface and can only take place normal to the surface plane. This results in a compressive hydrostatic swelling stress σ_h [8]:

$$\sigma_{h,sw} = -\frac{2\varepsilon_v E}{9(1-\nu)} = -\frac{2E}{9(1-\nu)}\kappa S, \quad \kappa = 0.97 \tag{2.4}$$

where E=72 GPa is Young's modulus and ν=0.17 is Poisson's ratio of silica. Consequently, it can be written

$$\sigma_{h,sw} = -\eta S = -\eta k C, \quad \eta = 18.7 \text{ GPa} \tag{2.5}$$

3. Stress effects on diffusivity

Due to diffusion, the concentrations of both molecular water, $C = [H_2O]$, and hydroxyl water, $S = [SiOH]$, decrease with increasing distance, z, from the surface. Stress can modify the effective diffusivity of water in silica in two different ways, directly through the activation free energy for diffusion and indirectly through its effect the equilibrium constant that determines the ratio of ≡SiOH to H_2O. In this report the first effect will be considered exclusively. The second effect is not unimportant and in fact has to be considered for very high stresses as for instance occur at the tips of loaded cracks in glass [7]. Its influence on surface concentrations is briefly addressed in the Appendix B.

The diffusivity D is a function of stress, commonly expressed by the hydrostatic stress component, σ_h. The stress-enhanced diffusivity is given by [10]

$$D = D_0 \exp\left[\frac{\sigma_h \Delta V_w}{RT}\right] \tag{3.1}$$

where D_0 denotes the value of the diffusivity in the absence of a stress. T is the absolute temperature in K; ΔV_w is the activation volume for stress-enhanced diffusion and R is the universal gas constant.

When an externally applied stress σ_{appl} and swelling stresses σ_{sw} are present simultaneously, the total hydrostatic stress is

$$\sigma_h = \sigma_{h,appl} + \sigma_{h,sw} \tag{3.2}$$

Since the swelling stress depends on the water concentration C, the diffusivity also depends on C, i.e. $D=D(C)$. The diffusion of molecular water is now governed by the partial differential equation for the uniaxial diffusion

$$\frac{\partial C}{\partial t} = \frac{\partial}{\partial z}\left[D(C)\frac{\partial C}{\partial z}\right] \tag{3.3}$$

Equation (3.3) was numerically solved using the *Mathematica* procedure *NDSolve* [11]. Fig. 1a shows water profiles as a function of time with the actual water concentrations normalized on the actual surface value $C(0)$.

The swelling stress related to a certain concentration C is

$$\sigma_{h,sw} = \sigma_{h,0}\frac{C}{C_0} \quad , \quad \sigma_{h,0} = \sigma_{h,sw}(C_0) \tag{3.4}$$

where the quantity $\sigma_{h,0}$ is the hydrostatic swelling stress value reached for $C=C_0$. For reasons of simplicity, we introduce a normalized dimensionless time τ and normalized depth coordinate ζ, defined by

$$\tau = \frac{h^2}{D_0} t \; ; \; \zeta = \frac{z}{\sqrt{D_0 t}} \tag{3.5}$$

With these abbreviations, eqs.(1.5) and (1.6) read

$$\frac{C(\zeta,\tau)}{C_0} = \text{erfc}\left[\frac{\zeta}{2}\right] - \exp[\zeta\sqrt{\tau} + \tau]\text{erfc}\left[\frac{\zeta}{2} + \sqrt{\tau}\right] \tag{3.6}$$

and

$$C(0,\, \tau)/C_0 = 1 - \exp[\tau]\text{erfc}[\sqrt{\tau}], \tag{3.7}$$

The blue curves in Fig. 1a show the concentration profiles in the absence of swelling. The red curves represent the profiles under swelling conditions. In both cases the bold curves show the limit cases for $t \to \infty$, i.e. under saturation conditions $C(0) = C_0$ [12].
In the absence of swelling, the widths of the diffusion profiles increase with the limit distribution described by

$$C = C_0 \,\text{erfc}\left(\frac{z}{2\sqrt{D_0 t}}\right) = C_0 \text{erfc}\left(\frac{\zeta}{2}\right) \tag{3.8}$$

The profile for t=0 or τ=0, introduced as the black dash-dotted curve, can be analytically computed. This concentration profile reads

$$\frac{C(\zeta,\tau)}{C(0)} = \exp\left[\frac{-\zeta^2}{4}\right] - \frac{\sqrt{\pi}}{2}\zeta \,\text{erfc}\left[\frac{\zeta}{2}\right] \tag{3.9}$$

From the condition

$$\exp\left[\frac{-\zeta^2}{4}\right] - \frac{\sqrt{\pi}}{2}\zeta \,\text{erfc}\left[\frac{\zeta}{2}\right] = \frac{1}{2} \tag{3.10}$$

the half width for $\tau \to 0$ follows by application of the *FindRoot*-routine of Mathematica [11] as $\zeta_{1/2}$=0.6995≅0.7.
The profiles under swelling conditions are shown by the red curves of Fig. 1a. With increasing normalized time, the curves become clearly steeper than those obtained without swelling.

In Fig. 1b the normalized depth $\zeta_{1/2}$ at which the water concentration decreased to the half of the surface value is plotted as a function of time. Whereas the diffusion zones in the absence of swelling stresses increase with time, they are clearly reduced with increasing time in the case of swelling included. This effect was already visible from Fig. 1a.

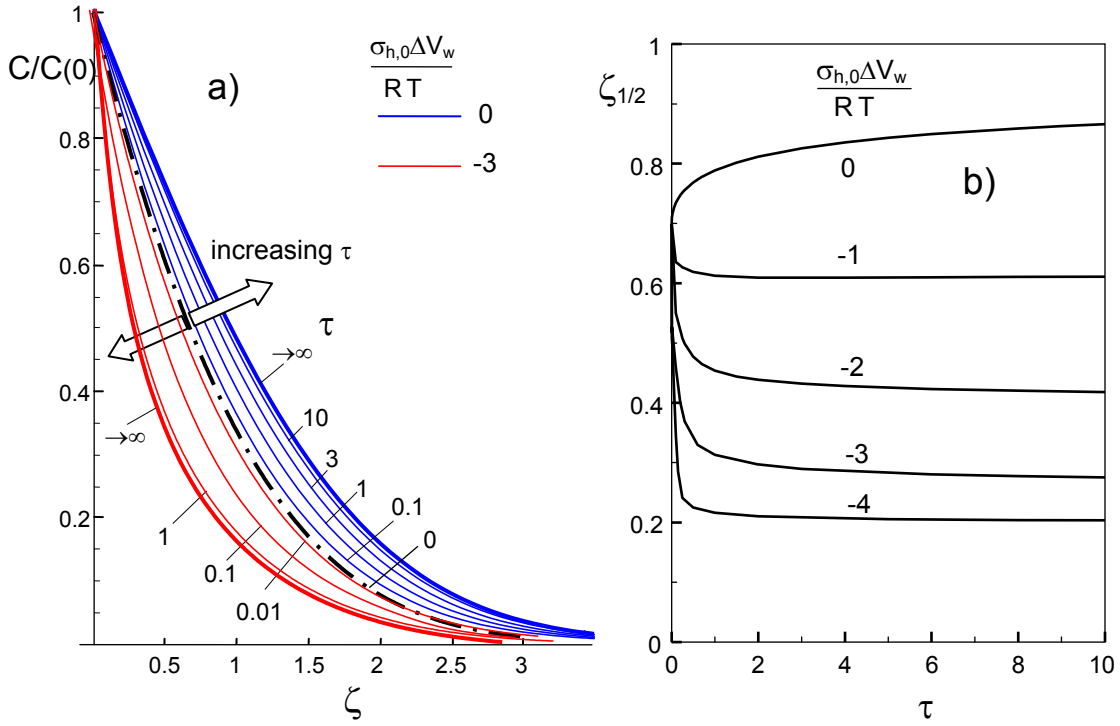

Fig. 1 a) Diffusion profiles as a function of normalized time without and with consideration of swelling stress effect on diffusivity, b) normalized diffusion depth (depth where $\zeta_{1/2}$=0.5) versus normalized time.

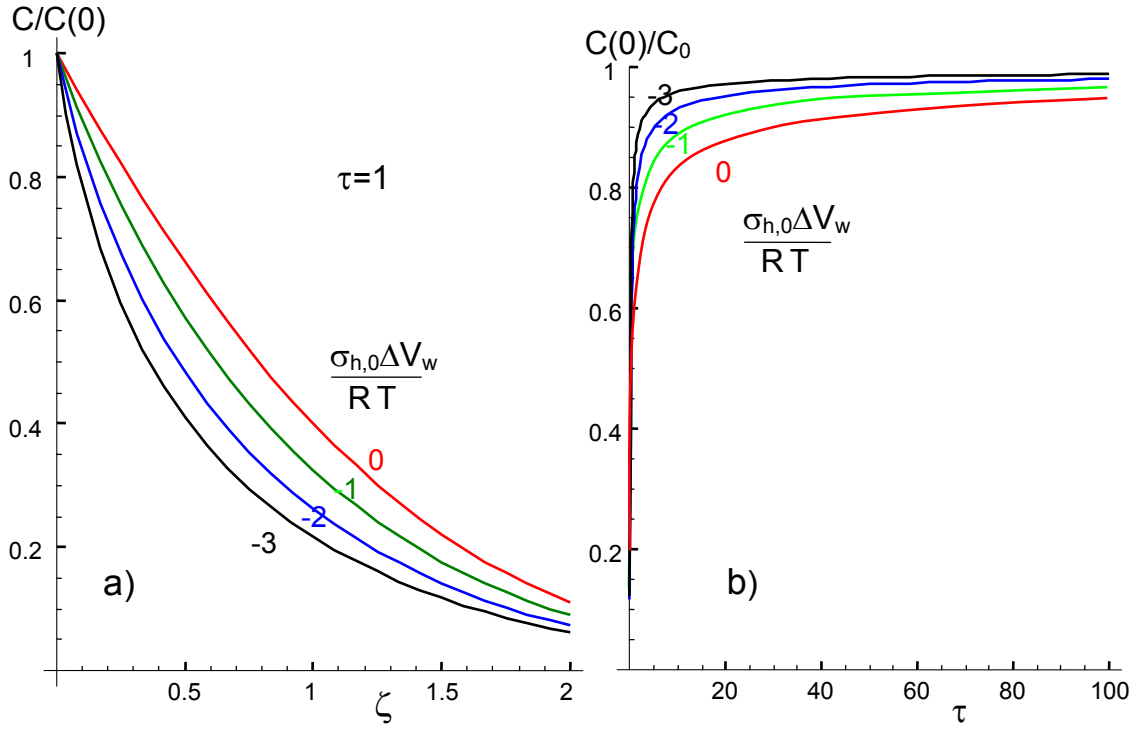

Fig. 2 a) Effect of the saturation stress $\sigma_{h,0}$, on the shape of the profiles, b) surface concentrations vs. time.

Fig. 2a shows the effect of the maximum swelling stress $\sigma_{h,0}$ on the shape of the concentration profiles and Fig. 2b represents the time-dependent surface concentration. The higher the compressive saturation swelling stress is, the earlier is saturation reached.

4 Comparison with experimental results from literature

4.1 Apparent diffusivity from diffusion profiles

Time-dependent diffusion profiles were measured by Davis and Tomozawa [13] in terms of the hydroxyl concentration *S* on silica hydrated in water vapour of 355mm Hg pressure at 350°C. The results, Fig. 3, showed reduced normalized diffusion depths with increasing soaking time. This behavior obviously agrees amazingly with the trend shown by the red curves in Fig. 1a. This can be interpreted as further evidence for the occurrence of compressive swelling stresses.

Approximate methods for the determination of the diffusivity from measurements of water profile and water uptake were proposed by Tomozawa and co-workers [13, 14]. Basis of their evaluation is the use of an equation that is only valid for a *constant surface concentration*, although the concentrations clearly increased with time:

$$C = C(0)\,\mathrm{erfc}\left(\frac{z}{2\sqrt{D_{eff}\,t}}\right) \tag{4.1}$$

One possibility for the computation of an "effective diffusivity" is via the measured depth $z_{1/2}$ at which the concentration decreased to 50% of the surface concentration.

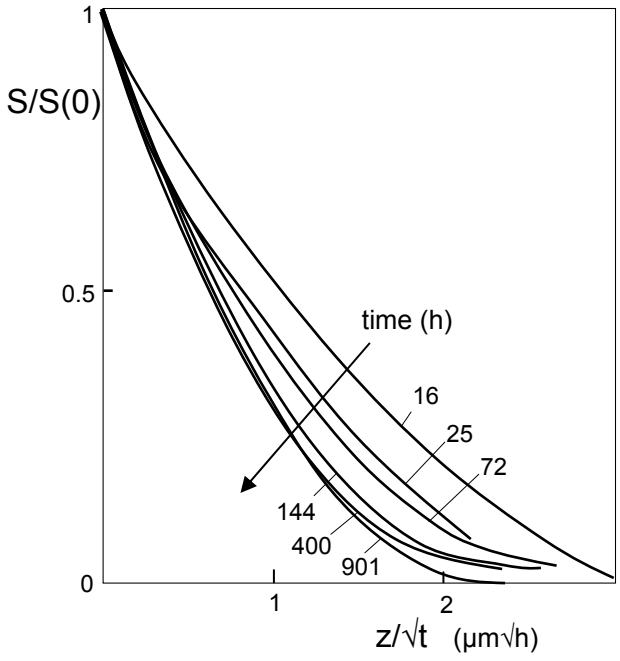

Fig. 3 Diffusion profiles by Davis and Tomozawa [13].

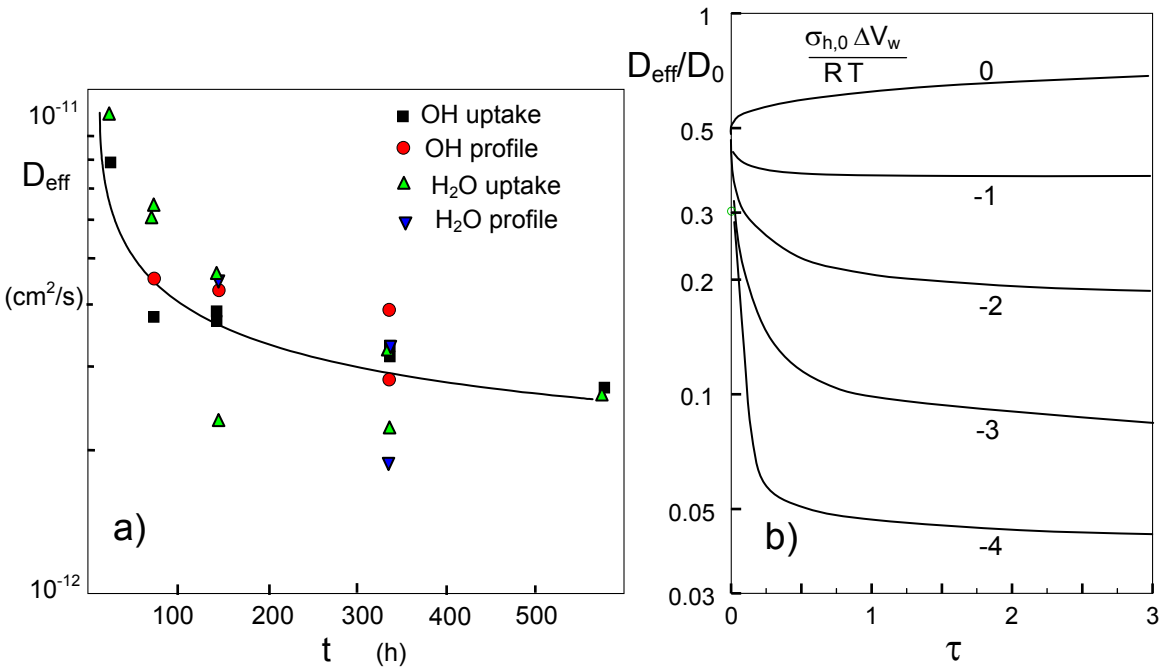

Fig. 4 a) Measurements of effective diffusivities by Oehler and Tomozawa [14] at 250°C and 39 bar water vapour pressure, b) effective diffusivity computed from the curves for the diffusion zone half-width $z_{1/2}$ of Fig. 1b.

An apparent diffusivity decreasing with time is clearly visible from experiments by Oehler and Tomozawa [14] measured at 250°C and 39 bar vapor pressure (Fig. 4a).

Computed apparent diffusivities obtained from the zone widths in Fig. 1b are shown in Fig. 4b. The same time dependency is obvious as obtained in the experiments by Oehler and Tomozawa [14].

4.2 Influence of externally applied stresses

4.2.1 Prediction of stress influence on water profiles

Beside the swelling stresses also externally applied stresses as present for instance in bending tests must affect the diffusion profiles. The diffusivity in the presence of a hydrostatic swelling stress term σ_h and an externally applied hydrostatic stress $\sigma_{h,ext}$ is given by

$$D = D_0 \exp\left[(\sigma_h + \sigma_{h,appl})\frac{\Delta V_w}{RT}\right] \tag{4.2}$$

For bending tests, the stresses are sufficiently constant within the range of the diffusion layers. In such tests, the upper and the lower surface of a bending bar show tensile and compressive stresses.

Concentration profiles computed with eqs.(3.1) and (3.3) are plotted in Fig. 5 and Fig. 6 for varied hydrostatic swelling terms $\sigma_{h,0}\Delta V_w/RT$ and varied time. It is obvious that in

all cases surface concentrations are smaller under externally applied tensile stresses than in the absence of such stresses. Compressive stresses cause an increase of water at the surface. The enlarged surface concentrations for compression decrease with respect to depth steeper than for tension. In deeper regions the concentrations under tension exceeds that for the compression side.

Since the swelling stresses $\sigma_{h,0}$ depend on the saturation concentration which is proportional to the vapour pressure and since the activation volume ΔV_w in eq.(3.1) is not known sufficiently, the parameter $\sigma_{h,0}\Delta V_w/RT$ was tentatively varied in Fig. 5.

Comparison of Fig. 5a to Fig. 5c shows clearly that the reason for the difference in surface concentrations is not caused by the swelling stresses since the effect occurs even in the absence of swelling, (Fig. 5a). With increasing swelling the difference at the surface is only slightly increased. From Fig. 5a we therefore have to conclude that the effect of the externally applied stresses on surface concentrations is due to the increase of water with time.

In Fig. 6 the time is varied for constant swelling $\sigma_{h,0}\Delta V_w/RT$=-2. The results indicate that for short times the concentration differences at the surfaces are larger than for longer times. For $\tau \rightarrow \infty$ the differences must of course disappear completely because then the water concentration reaches saturation independent of the applied stress.

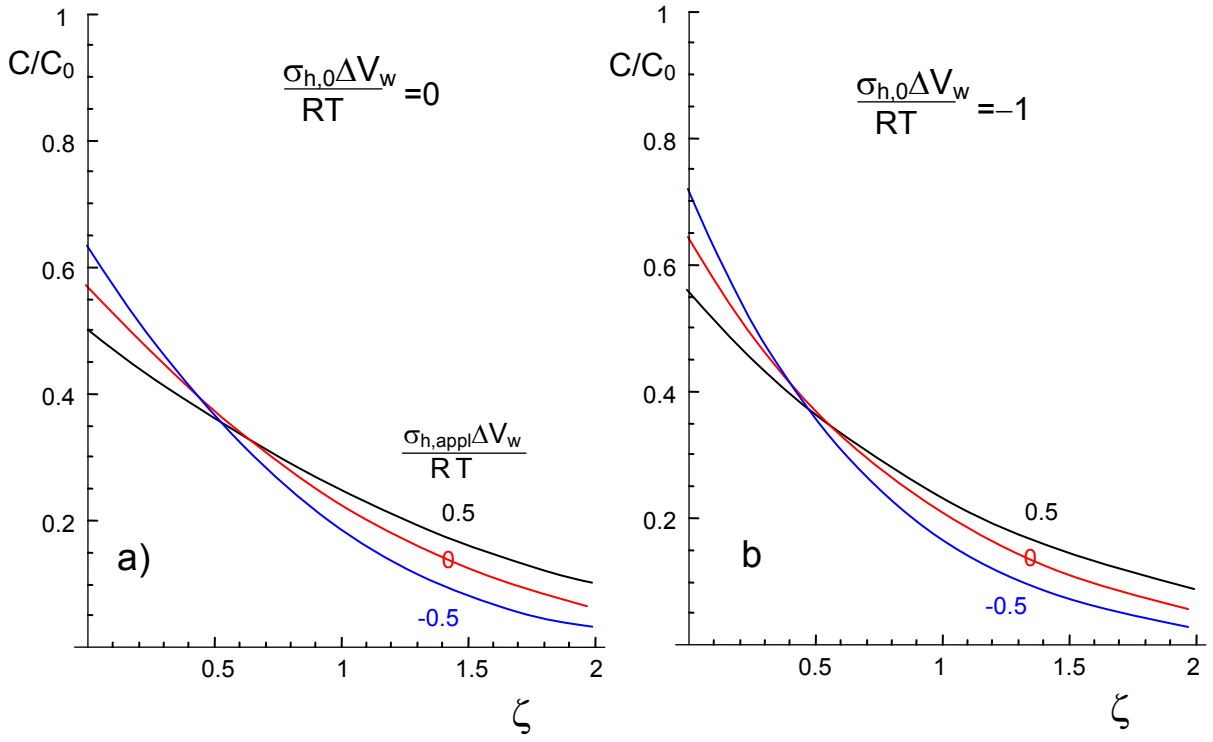

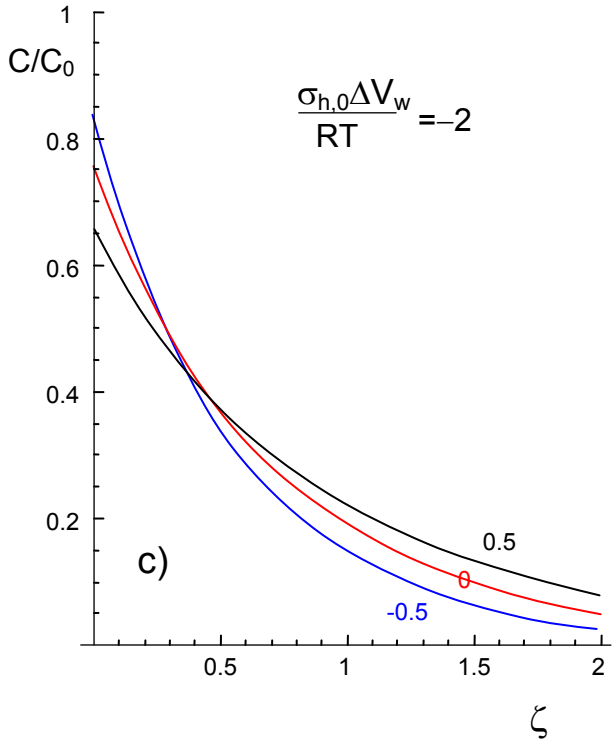

Fig. 5 Diffusion profiles under externally applied stresses; effect of swelling (soaking time, τ=1).

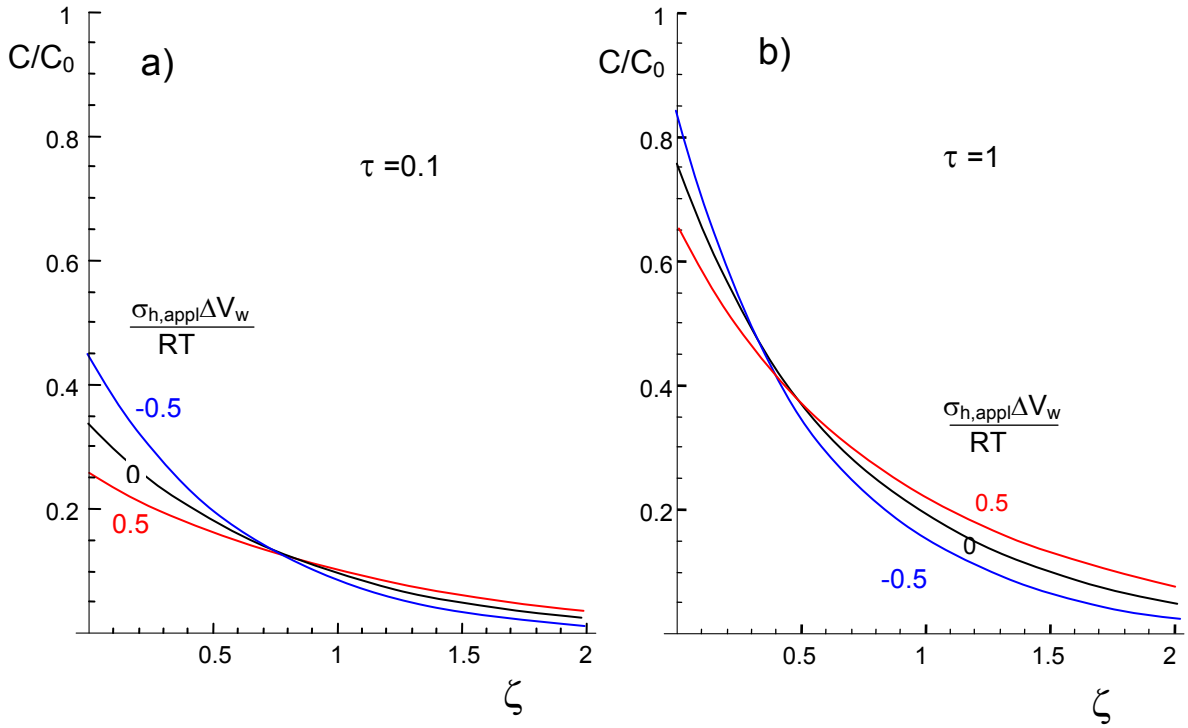

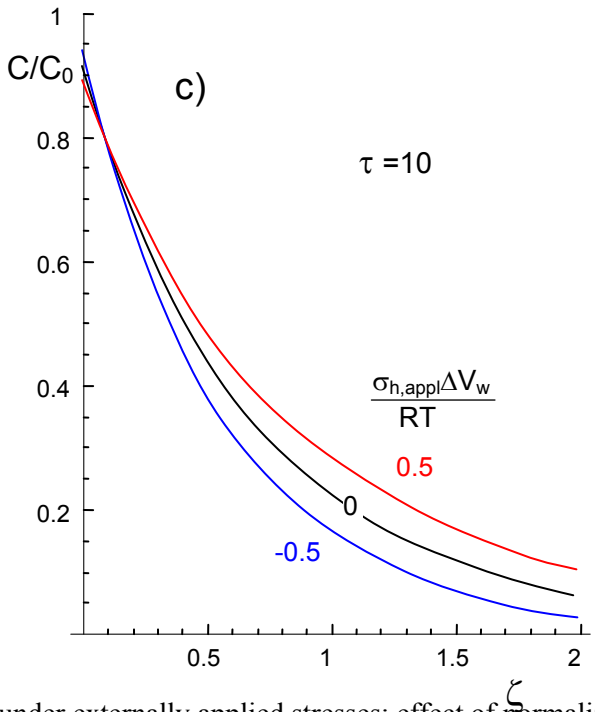

Fig. 6 Diffusion profiles under externally applied stresses; effect of normalized soaking time, t, for $\sigma_{h,0}\Delta V_w/RT$=-2.

For simplified evaluations, a series expansion of the water concentration at the surface may be used that reads

$$\frac{C(\sigma,\tau)}{C_0}=\frac{C_{\sigma=0}}{C_0}-\left(\sqrt{\frac{\tau}{\pi}}-\tau\left(1-\frac{C_{\sigma=0}}{C_0}\right)\right)\left(\frac{D}{D_0}-1\right)+O\left(\frac{D}{D_0}-1\right)^2 \tag{4.3}$$

Equivalent to (4.3) it is

$$\frac{C(\sigma,\tau)}{C_0}=\frac{C_{\sigma=0}}{C_0}-\left(\sqrt{\frac{\tau}{\pi}}-\tau\exp(\tau)\operatorname{erfc}(\sqrt{\tau})\right)\left(\frac{D}{D_0}-1\right)+O\left(\frac{D}{D_0}-1\right)^2 \tag{4.4}$$

In the case of bending tests the difference of the concentrations on the two surfaces is

$$\frac{C_{\sigma>0}-C_{\sigma<0}}{C_0}=-\left(\sqrt{\frac{\tau}{\pi}}-\tau\left(1-\frac{C_{\sigma=0}}{C_0}\right)\right)\left(\frac{D_{\sigma>0}}{D_0}-\frac{D_{\sigma<0}}{D_0}\right)+\ldots \tag{4.5}$$

$$\frac{C_{\sigma>0}-C_{\sigma<0}}{C_0}=-\left(\sqrt{\frac{\tau}{\pi}}-\tau\exp(\tau)\operatorname{erfc}(\sqrt{\tau})\right)\left(\frac{D_{\sigma>0}}{D_0}-\frac{D_{\sigma<0}}{D_0}\right)+\ldots \tag{4.6}$$

The stress effect on the surface concentration can simply be summarized:
Under *tensile stresses* the diffusivity is increased and diffusion is enhanced. This must result in

- an increased zone thickness compared to the tests without externally applied stresses.
- Due to the higher diffusivity under tensile stresses, the water diffusion into the bulk material is also increased. Since the water entrance from the environment into the surface is limited by the finite value of h, the concentration of water at the surface must decrease.

Under *compressive stresses* the diffusivity is reduced. This results in a reduced penetration depth and an increased surface concentration.

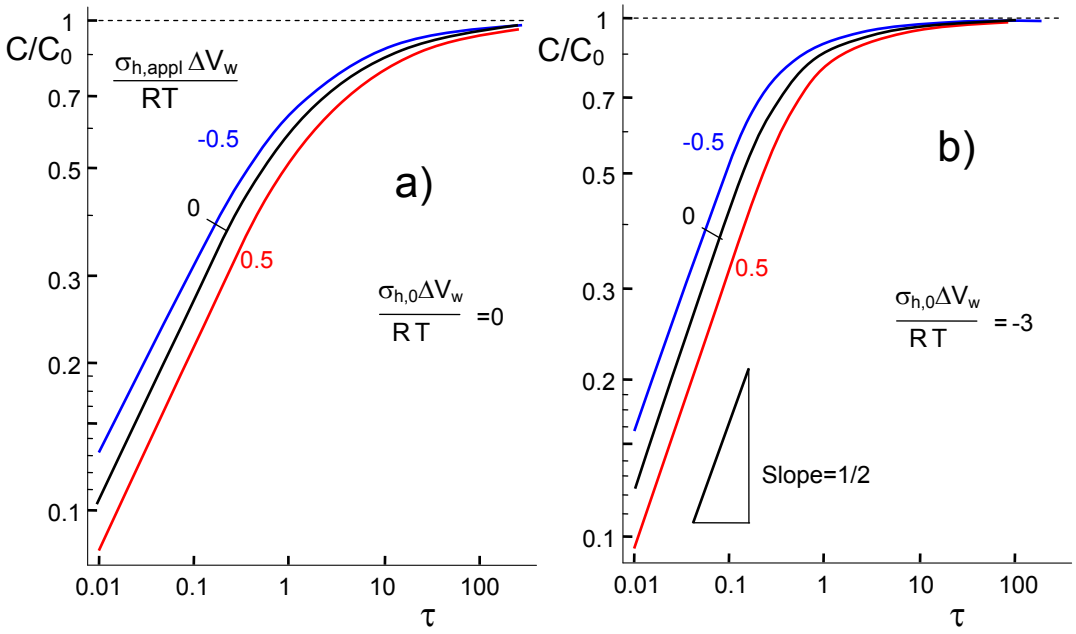

Fig. 7 Water concentration at the surface as a function of time under externally applied and swelling stress, a) for negligible swelling, $\sigma_{h,0}=0$; b) with swelling included, $\sigma_{h,0}\neq 0$.

The water concentration at the surface is plotted in Fig. 7 as a function of applied stress and time τ with the swelling stress varied. In Fig. 7a the case of negligible swelling stresses, $\sigma_{h,0}=0$, is plotted. Figure 7b shows the effect of considerable swelling. For short normalized time τ the surface water concentration is proportional to $\sqrt{\tau}$ and for large time it equals the concentration prescribed by the environment, C_0:

$$\frac{C}{C_0}=\begin{cases}\propto\sqrt{\tau} & \tau\to 0\\ 1 & \tau\to\infty\end{cases} \tag{4.7}$$

It is visible that the water concentration on the tensile side of a bending specimen is lower than the concentration on the compressive side. This difference disappears with increasing time. For $\tau\to\infty$ the concentration is on both sides equal C_0. Under swelling stresses the change from the $\sqrt{\tau}$-dependency to $C/C_0=1$ is more abrupt.

4.2.2 Results by Nogami and Tomozawa

Figure 8a shows experimental results on bending bars by Nogami and Tomozawa [15] at 190°C carried out after 300h treatment in water atmosphere at 12 bars water vapour pressure. Measurements were carried out on the tensile and compression side under load and in an additional test also on unstressed bars.

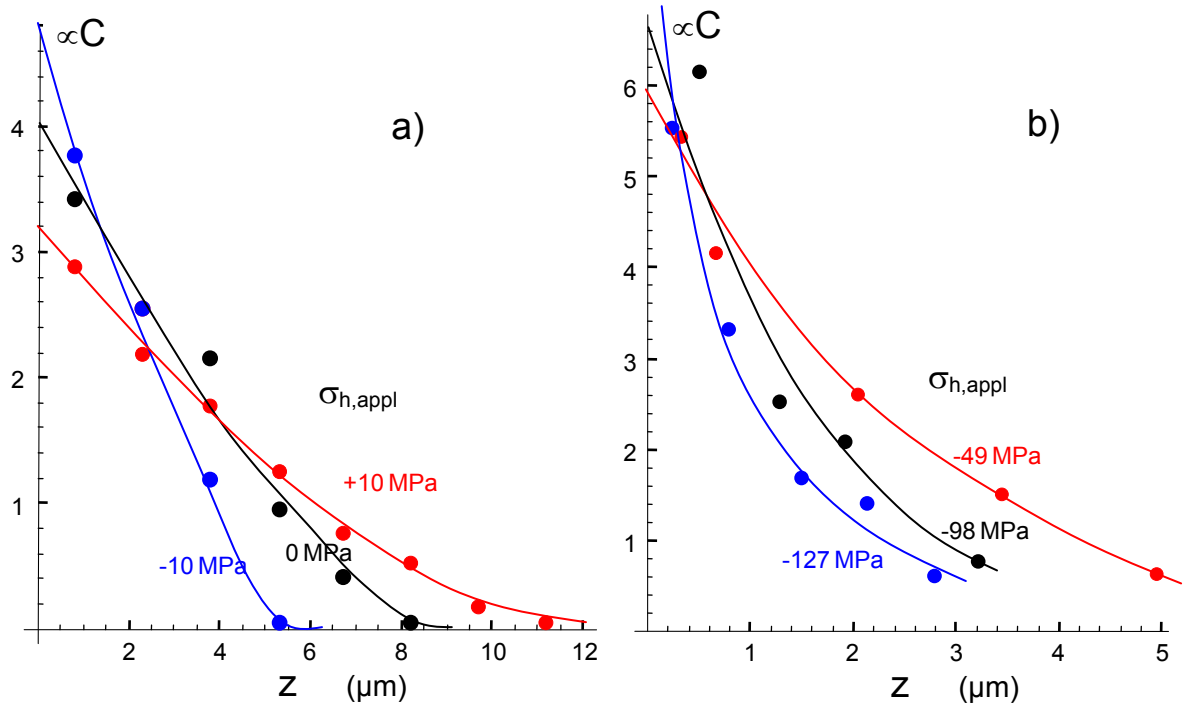

Fig. 8 Concentration profiles by Nogami and Tomozawa [15] as a function of the hydrostatic stress, a) bending bars for silica at 192°C (water vapour pressure: 12.3 bars), b) externally pressurized specimens at 350°C (water vapour pressure: 25 bars), *C*: in absorption coefficients (1/mm).

In Fig. 8b similar results at 350°C are shown for 5h soaking (water atmosphere at 25 bars). In this case, Nogami and Tomozawa [15] applied hydrostatic pressures directly. The results of Fig. 8 completely confirm the computed curves in Fig. 5 and Fig. 6. The effective activation volume was experimentally determined in [15] as ΔV_w =170 cm^3/mol for 192°C and 72 cm^3/mol at 350°C.

4.2.3 Results by Davis and Tomozawa

Figure 9a shows hydroxyl concentration data in mass units under water saturation pressure as could be computed from measurements by Zouine et al. [12] using the equilibrium equation from Wiederhorn et al. [8]. The straight line introduced in this plot reads

$$S_{sat} = 0.000265 \exp(0.0143\,\theta) \tag{4.8}$$

with the temperature θ in °C. An extrapolation to θ=250°C results in the saturation concentration of S=0.94 wt%. The corresponding hydrostatic swelling stress term at a free surface is given by eq.(2.5): $\sigma_{h,0}$= -177 MPa.

Consequently, it holds for 250°C:

$$\frac{\sigma_{h,0}\Delta V_w}{RT} = -0.0407\,\Delta V_w \tag{4.9}$$

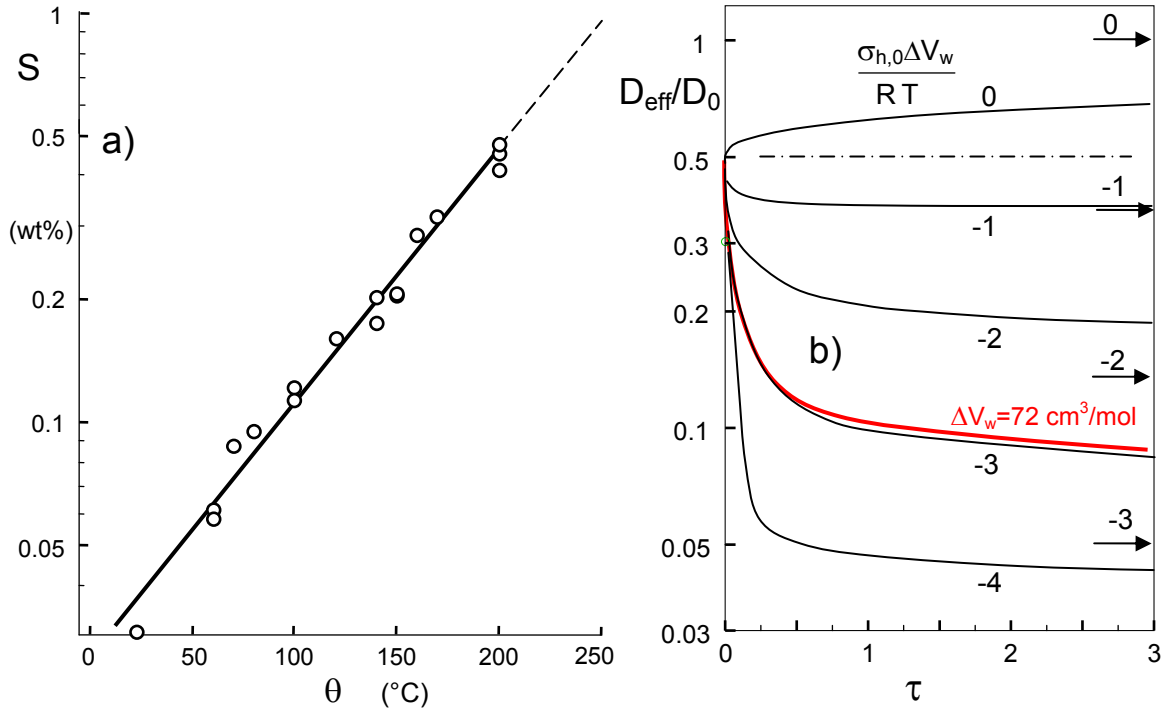

Fig. 9 a) Concentration of hydroxyl water at silica surfaces under saturation pressure by Zouine et al. [12], b) results of Fig. 4b together with the curve related to the effective volume ΔV_w=72 cm^3/mol (red curve) as was derived by Nogami and Tomozawa [15], arrows: limit values for $\tau\to\infty$.

In Fig. 9b the results of Fig. 4b are shown once more together with the parameter chosen for the results obtained by Nogami and Tomozawa [15], namely, ΔV_w =72 cm^3/mol (the value of ΔV_w =170 cm^3/mol seems to be extremely large). For the parameter (4.9) it results: $\sigma_{h,0}\Delta V_w/RT$= –2.93.

The ratio of diffusivities for the asymptotic limit, $\tau\to\infty$, are given by the arrows to the right. This limit case has to be expected either for liquid water in contact with silica surfaces or for water vapour environment after extremely long times t.

Finally, Fig. 10 illustrates the ratio D_{eff}/D_0 from Fig. 9 as a function of the swelling parameter $\sigma_{h,0}\Delta V_w/RT$ by the circles. The dash-dotted straight line represents eq.(3.1). The red arrows indicate the activation volumes suggested by Nogami and Tomozawa [15]. For strongly negative swelling parameters, the integration procedure for the nu-

merical solution of eq.(3.3) becomes rather unstable. A rough estimation for the very large value of 170 cm^3/mol needs an extrapolation of computed results. Such an extrapolation is tentatively shown by the dashed extension of the computed data curve.

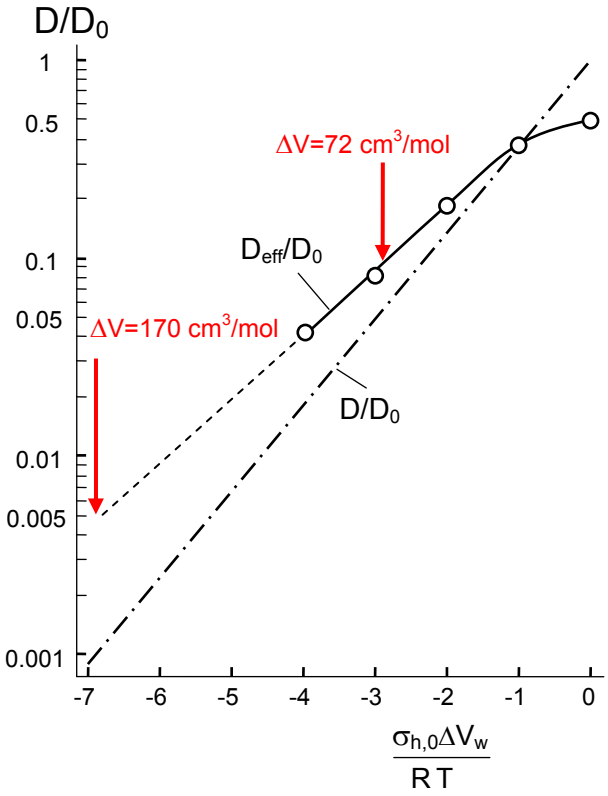

Fig. 10 Diffusivity ratio of D_{eff}/D_0 from Fig. 9b for normalized time τ=3 versus the swelling parameter $\sigma_{h,0}\Delta V_w/RT$ (symbols) compared with the diffusivity ratio D/D_0 according to eq.(3.1) (dash-dotted line); the dashed line is tentatively introduced for extrapolations.

4.2.4 Results by Agarwal et al.

Hydrogen concentrations close to silica surfaces were reported by Agarwal et al. [16]. These authors used the nuclear reaction analysis (NRA) on water profiles in specimens that were hot-water soaked at 250°C under 355 Torr vapour pressure. These results are represented in Fig. 11a. The water content under pressure (compressive side of a bent specimen) is always higher than under tension. This is in complete agreement with the data by Nogami and Tomozawa [15] and shows the same behaviour as the predictions given in Figs. 6 and 7.

Since no surface concentrations are given in [16], we plotted the data at 0.12 µm below the surface versus soaking time in Fig. 11b. The slopes of the regression lines are

0.588 [0.553, 0.624] for tension, +60 MPa

0.495 [0.467, 0.523] for compression, –60 MPa

with the 90% Confidence Intervals in brackets.

These results roughly fulfil the surface predictions for short times, namely $C/C_0 \propto \sqrt{t}$. This result indicates that even the longest soaking time of 16h is far away from saturation.

When stress-enhanced swelling is taken into consideration, the influences of tension and compression will change for long soaking time. This is outlined in the Appendix B.

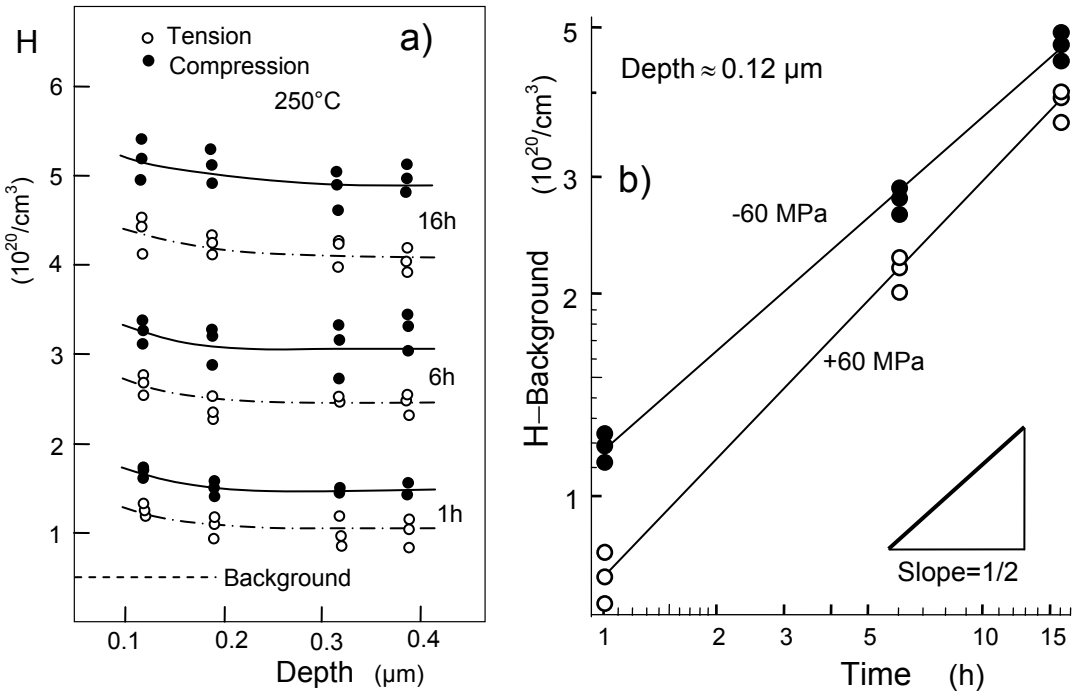

Fig. 11 a) Water concentration below the surface at 250°C and 355Torr vapour pressure under bending stresses of 60MPa, b) data at a depth of 0.12 μm below the surface plotted vs. soaking time.

Conclusions

There are several important findings from the computation of diffusion profiles for water vapour soaked silica when the surface condition, eq.(1.3), is applied. The results plotted in Figs. 1 and 2 show that the existence of a finite *mass transfer coefficient* or *reaction parameter h* affects the shape of the profiles. Whereas in liquid water the profile of the water distribution zone can be described by the well-known dependency

$$C \propto \operatorname{erfc}[z/(2\sqrt{Dt})],$$

[12], the concentration distribution for a vapour environment deviates.

- In the absence of swelling stresses, the steepness of the normalized water diffusion profile, given by the continuous curves in Fig. 1a, decreases with increasing normal-

ized time. The concentration profile given by the above equation is reached after an infinite normalized time;

- In presence of swelling stresses in the diffusion layer, the water profiles become steeper with increasing time as is visible from the dashed curves in Fig. 1a;

Measured water concentration profiles, Fig. 3, clearly show the effect of time on the shape of the diffusion profiles. The increasing curve steepness with increasing time is evidence for the presence of compressive swelling stresses.

From the depths $z_{1/2}$ at which the water concentration decreases to 50% of the surface value an apparent diffusivity, D_{eff}, was defined by Davis and Tomozawa [13] via $z_{1/2} = \sqrt{D_{eff} t}$. The apparent diffusivity D_{eff}, Fig. 1b, decreases with time and swelling stresses. This result is in best agreement with the experimental observations by Davis and Tomozawa [13] and by Öhler and Tomozawa [14], Fig. 4a. This also shows that swelling of silica is present.

From our computations, the results by Nogami and Tomozawa [15] became easily understandable. The same holds for equivalent results by Agarwal et al. [16], Fig. 11.

APPENDIX A:

A1 Diffusion differential equation and approximations

Introducing (1.2) in (1.4) gives

$$\frac{\partial C}{\partial t} = \frac{\partial}{\partial z}\left(D_C \frac{\partial C}{\partial z} \right) - \frac{1}{2}\frac{\partial (kC)}{\partial t} \tag{A1}$$

or

$$\frac{\partial C}{\partial t} = \frac{\partial}{\partial z}\left(D_C \frac{\partial C}{\partial z} \right) - \tfrac{1}{2} k \frac{\partial C}{\partial t} - \tfrac{1}{2} C \frac{\partial k}{\partial t} \tag{A2}$$

Several steps can be made to simplify these equations:

- Under the assumption of a stress-independent equilibrium constant, $k=k_0$, we obtain

$$\frac{\partial C}{\partial t} \cong \frac{\partial}{\partial z}\left(D_C \frac{\partial C}{\partial z} \right) - \tfrac{1}{2} k_0 \frac{\partial C}{\partial t} \Rightarrow \frac{\partial C}{\partial t}(1 + \tfrac{1}{2} k_0) = \frac{\partial}{\partial z}\left(D_C \frac{\partial C}{\partial z} \right)$$

$$\Rightarrow \frac{\partial C}{\partial t} = \frac{\partial}{\partial z}\left(D \frac{\partial C}{\partial z} \right) \quad , D = \frac{D_C}{1 + \tfrac{1}{2} k_0} \tag{A3}$$

defining an effective diffusivity D.

- Assuming in addition a stress-independent diffusivity, D=const., yields in the simplest approximation

$$\frac{\partial C}{\partial t} \cong D \frac{\partial^2 C}{\partial z^2} \tag{A4}$$

as was used in [2].

A2 A semi-analytical approach

The numerical effort for the solution of the diffusion equation, eq.(3.3), is hardly manageable in presence of swelling stresses. An approximate analytical solution can be obtained following the general procedure usual in perturbation theory. If we consider the diffusivity $D(C)$ as the disturbance parameter, perturbation theory suggests to solve the problem for the case of $D(0)=D_0$ and to insert the disturbance parameter into this solution. The disturbed solution is then obtained by introducing $D(C)$ instead of D_0 into the undisturbed solution. Since the analytical solution of the undisturbed problem, here denoted as the first-order solution $C^{(1)}$ is given by

$$\frac{C^{(1)}}{C_0} = \mathrm{erfc}\left[\frac{z}{2\sqrt{D_0 t}}\right] - \exp\left[\frac{h}{D_0}z + \frac{h^2}{D_0}t\right]\mathrm{erfc}\left[\frac{z}{2\sqrt{D_0 t}} + h\sqrt{\frac{t}{D_0}}\right] \tag{A5}$$

the analytical second-order solution $C^{(2)}$ simply reads

$$\frac{C^{(2)}}{C_0} = \mathrm{erfc}\left[\frac{z}{2\sqrt{D(C^{(1)})t}}\right] - \exp\left[\frac{h^2}{D(C^{(1)})}z + \frac{h^2}{D(C^{(1)})}t\right]\mathrm{erfc}\left[\frac{z}{2\sqrt{D(C^{(1)}t}} + h\sqrt{\frac{t}{D(C^{(1)})}}\right] \tag{A6}$$

with the diffusivity, eq.(3.1), taken at the local- and time-dependent concentration $C=C^{(1)}$.

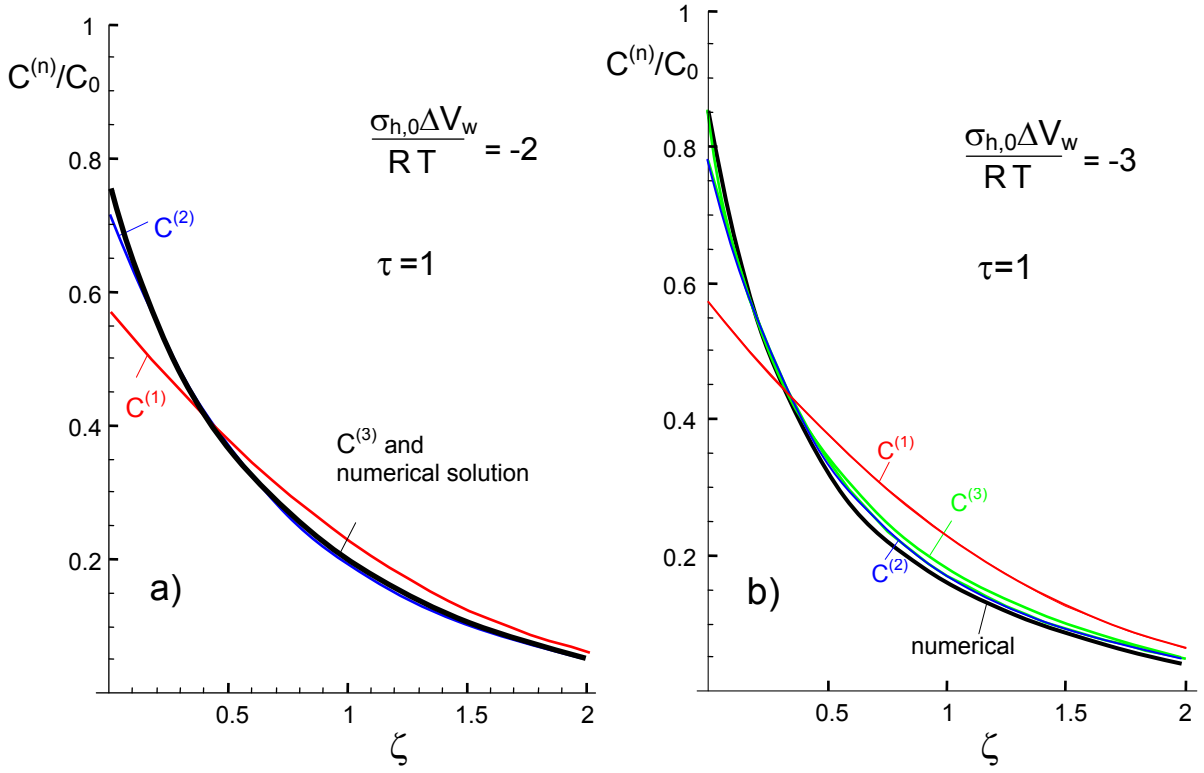

Fig. A1 a), b) Semi-analytical solutions $C^{(n)}$ compared with numerical results for $t\times h^2/D_0=1$.

Higher iteration solutions are possible by introducing $D(C^{(n)})$ on the right-hand side, resulting in $C^{(n+1)}$, etc.

$$\frac{C^{(n+1)}}{C_0} = \mathrm{erfc}\left[\frac{z}{2\sqrt{D(C^{(n)})t}}\right] - \exp\left[\frac{h}{D(C^{(n)})}z + \frac{h^2}{D(C^{(n)})}t\right]\mathrm{erfc}\left[\frac{z}{2\sqrt{D(C^{(n)}t}} + h\sqrt{\frac{t}{D(C^{(n)})}}\right] \tag{A7}$$

A comparison of the perturbation solutions and the numerical results from eq.(3.3) is given in Fig. A1. Whereas for $\sigma_{h,0}\Delta V_w/RT = -2$ (Fig. A1a) the iteration solution $C^{(3)}$ is in complete agreement with the numerical solution, first small deviations are visible for $\sigma_{h,0}\Delta V_w/RT = -3$, Fig. A1b. Therefore, it is suggested to use the perturbation solution only for not too strong swelling stresses.

APPENDIX B:

B Stress-enhanced equilibrium constant

B1 Low temperature <500°C

Because of the principle of Le Chatelier [17], the equilibrium of reaction (1.1) and the hydroxyl concentration depend on stresses. Whereas in the preceding derivations the influence of swelling stresses was considered exclusively, here the effect of externally applied *uniaxial* stresses σ_{appl} is taken into account at temperatures < 500°C. Then the equilibrium constant k reads in terms of the hydrostatic part of the applied stresses, $\sigma_{h,appl}=\sigma_{appl}/3$, and the hydrostatic part of the swelling stresses, $\sigma_{h,sw}$,

$$k = k_{1,0} \exp\left[\frac{(\frac{1}{3}\sigma_{appl} + \sigma_{h,sw})V_1}{RT} \right], \tag{B1}$$

The parameter $k_{1,0}$ *is* the equilibrium constant in the absence of any stress. V_1 is the increase in partial molar volume during the reaction. It is of importance to note that the swelling stress, $\sigma_{h,w}$ is proportional to the hydroxyl concentration S as given by eq.(2.5).

$$k = k_{1,0} \exp\left[\frac{(\frac{1}{3}\sigma_{appl} - \eta k C)V_1}{RT} \right], \tag{B1a}$$

This is an implicit equation with k occurring on the left side as well as in the argument of the exponential function. The explicit solution of (B1a) reads

$$k = \frac{RT}{C\eta V_1} \mathrm{PLog}\left[\frac{\eta k_{1,0} C V_1}{RT} \exp\left(\frac{\frac{1}{3}\sigma_{appl} V_1}{RT} \right) \right], \tag{B1b}$$

with the *product logarithm* or Lambert *W* function PLog. Finally, eq.(1.4) is rewritten as

$$\frac{\partial C}{\partial t} = \frac{\partial}{\partial z}\left(D_C \frac{\partial C}{\partial z} \right) - \frac{1}{2}\frac{RT}{\eta V_1} \times \frac{\partial}{\partial t}\left(\mathrm{PLog}\left[\frac{\eta k_{1,0} C V_1}{RT} \exp\left(\frac{\frac{1}{3}\sigma_{appl} V_1}{RT} \right) \right] \right) \tag{B2}$$

again obtained by using *NDSolve* of *Mathematica* [11].

Since water concentration measurements are mostly performed via the IR band (3670/cm) for the hydroxyl species, *S*, it is of advantage for predictions to give *S* as a function of time. The result of eq.(A2), given as molecular water concentration $C(t)$, reads according to eq.(B1):

$$S = C \times k_{1,0} \exp\left[\frac{(\frac{1}{3}\sigma_{appl} + \sigma_{h,sw})V_1}{RT}\right], \tag{B3}$$

Figure B1a shows the surface concentration *S* normalized on $(C_0 \times k_{1,0})$. The hydroxyl water concentration shows for short time τ a concentration proportional to $(\text{time})^{1/2}$. The water concentration under compressive stresses is larger than in tension for short times. After longer time, the concentration on the tensile side becomes larger than that on the compression side.

To our knowledge, there are no results available for very long times, $t >> 16$h, for which the predicted change of the stress effect would be expected. An indication for an expected intersection of the tensile and compression results might by identified by the different slopes of the two lines in Fig. 11b.

B2 High temperature >500°C

The equilibrium at high temperatures is given by

$$k_2 = \frac{S^2}{C} \tag{B4}$$

with now

$$S = \sqrt{C\,k_{2,0}} \exp\left[\frac{(\frac{1}{3}\sigma_{appl} + \sigma_{h,sw})V_2}{RT}\right] \tag{B5}$$

Consequently, it holds instead of eq.(1.2)

$$\frac{\partial C}{\partial t} = \frac{\partial}{\partial z}\left(D_C \frac{\partial C}{\partial z}\right) - \frac{1}{2}\frac{\partial(\sqrt{k_2 C})}{\partial t} \tag{B6}$$

The numerical solution of this differential equation is plotted in Fig. B1b as $S(\tau)$. The slope in this diagram is ¼ instead of ½ as was obtained in Fig. B1a.

Measurements by Agarwal et al. [16] at 650°C and 355 Torr water vapour pressure are plotted in Fig. B2. These data confirm clearly the effect of higher water concentration under compression for short time and higher water concentration in tension for longer times.

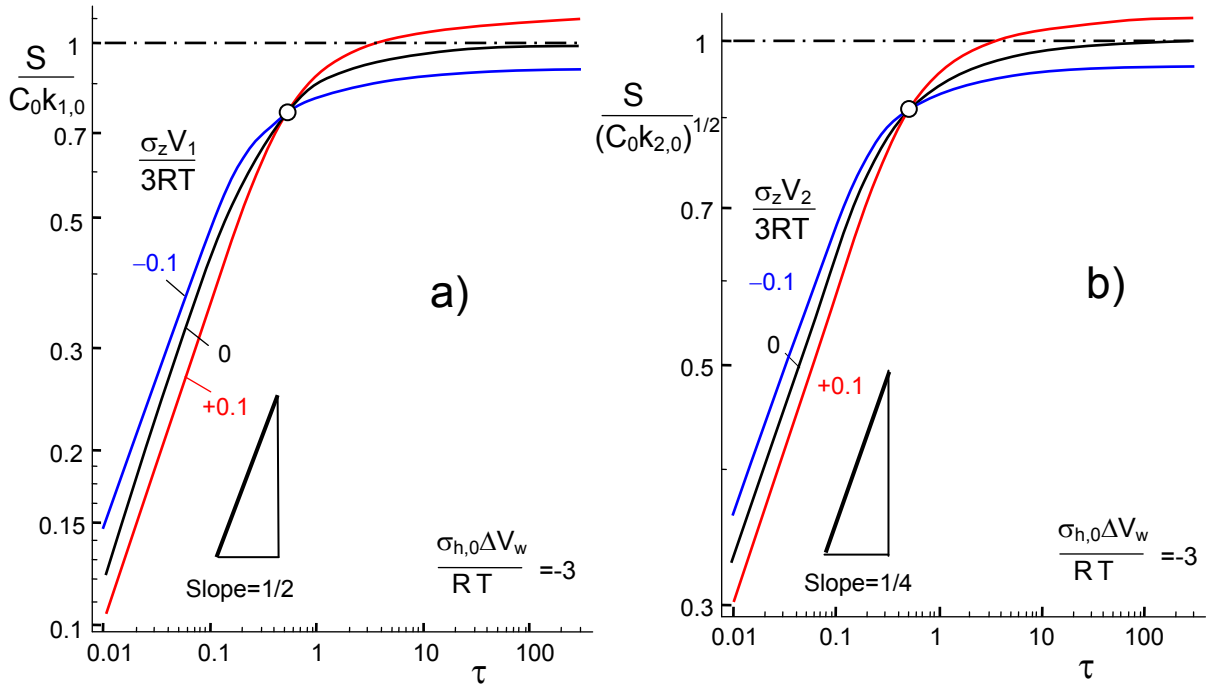

Fig. B1 a) Hydroxyl concentrations for stress-enhanced hydroxyl water at a silica surface for temperatures <450-500°C computed with a parameter of $|\sigma_{appl}|/3\times V_w/RT=0.5$, b) for stress-enhanced hydroxyl water at a silica surface for temperatures >450-500°C.

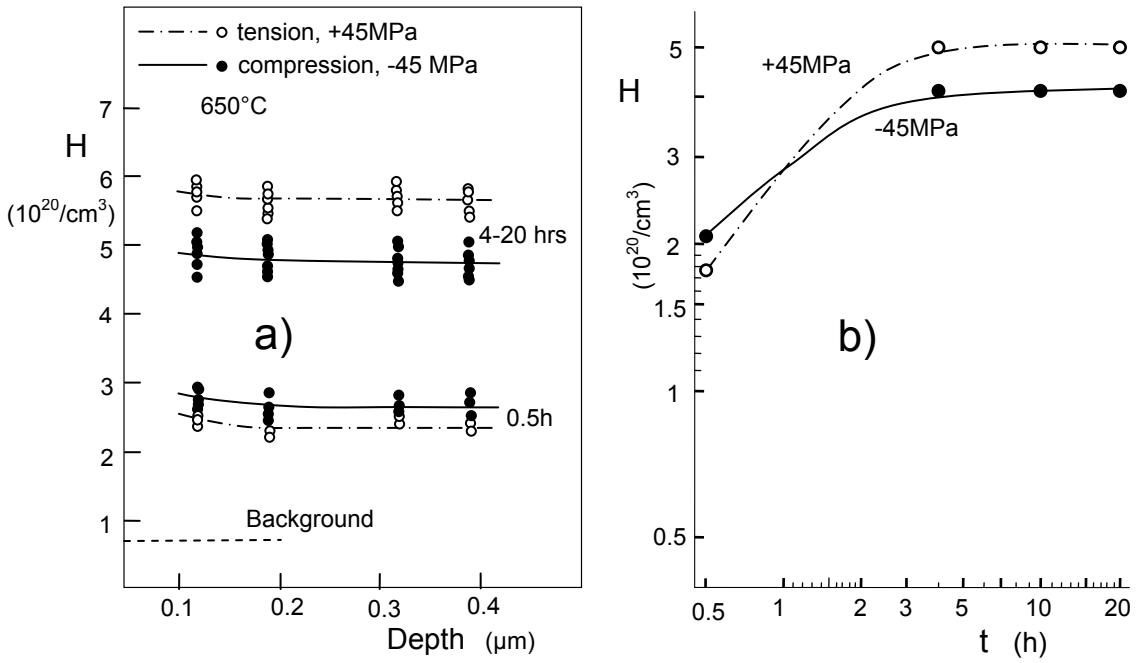

Fig. B2 a) Hydrogen concentration below the surface at 650°C and 355Torr vapour pressure under bending stresses of 45MPa, b) H-concentration in 0.12μm depth versus time.

References

1 Doremus, R.H., Diffusion of water in silica glass, J. Mater. Res., **10**(1995), 2379-2389.

2 T. Fett, S.M. Wiederhorn, Silica in humid air environment, (I): Diffusion in the absence of stresses, Report KIT-SWP 11, 2013, Karlsruhe.

3 R.H. Doremus, Diffusion of Reactive Molecules in Solids and Melts, Wiley, 2002, NewYork.

4 J. Crank, *The Mathematics of Diffusion,* Oxford University Press, Oxford OX2 6DP (1956)

5 Carslaw, H.S., Jaeger, J.C. Conduction of heat in solids, 2nd ed. 1959, Oxford Press, London).

6 Shelby, J.E., "Density of vitreous silica," J. Non-Cryst. **349** (2004), 331-336.

7 S.M. Wiederhorn, T. Fett, G. Rizzi, S. Fünfschilling, M.J. Hoffmann and J.-P. Guin, "Effect of Water Penetration on the Strength and Toughness of Silica Glass," *J. Am. Ceram. Soc.* **94** [S1] S196-S203 (2011)

8 S. M. Wiederhorn, F. Yi, D. LaVan, T. Fett, M.J. Hoffmann, Volume Expansion caused by Water Penetration into Silica Glass, J. Am. Ceram. Soc. **98** (2015), 78-87.

9 S. M. Wiederhorn, M. J. Hoffmann, T. Fett, Swelling strains from density measurements, Scientific Working Papers **38**, 2015, KIT Scientific Publishing, Karlsruhe.

10 P.G. Shewman, Diffusion in Solids, McGraw-Hill, New York, 1963.

11 *Mathematica*, Wolfram Research, Champaign, USA.

12 A. Zouine, O. Dersch, G. Walter and F. Rauch, "Diffusivity and solubility of water in silica glass in the temperature range 23-200°C," *Phys. Chem. Glass: Eur. J. Glass Sci and Tech. Pt. B*, **48** [2] 85-91 (2007).

13 Davis, K.M., Tomozawa, M., Water diffusion into silica glass: structural changes in silica glass and their effect on water solubility and diffusivity, J. Non-Cryst. Sol. **185**(1995), 203-220.

14 Oehler, A., Tomozawa, M., Water diffusion into silica glass at a low temperature under high water vapor pressure, J. Non-Cryst. Sol. **347**(2004) 211-219.

15 M. Nogami, M. Tomozawa, Diffusion of water in high silica glasses at low temperature, Phys. and Chem. of Glasses **25**(1984), 82-85.

16 A. Agarwal, M. Tomozawa, W. A. Lanford, Effect of stress on water diffusion in silica glass at various temperatures, J. Non-Cryst. **167**(1994), 139-148.

17 H. Le Chatelier, *C.R. Acad. Sci. Paris* **99**(1884), 786.

KIT Scientific Working Papers
ISSN 2194-1629

www.kit.edu